2023-10

Zinc oxide nanoparticles disrupt development and function of the olfactory sensory system impairing olfaction-mediated behaviour in zebrafish

Takesono, Aya

10.1016/j.envint.2023.108227
Environment International
Elsevier BV

Zinc Oxide Nanoparticles Disrupt Development and Function of the Olfactory Sensory System Impairing Olfaction-Mediated Behaviour in Zebrafish

Aya Takesono[1*], Sylvia Dimitriadou[1], Nathaniel J. Clark[2], Richard D. Handy[2], Sulayman Mourabit[1], Matthew J. Winter[1], Tetsuhiro Kudoh[1] and Charles R. Tyler[1*]

1: Biosciences, College of Life and Environmental Sciences, University of Exeter, Exeter, Devon, EX4 4QD, United Kingdom.

2: Faculty of Science and Engineering, School of Biological and Marine Sciences, University of Plymouth, Drake Circus, Plymouth, PL4 8AA, United Kingdom.

*Corresponding authors: Aya Takesono (A.Takesono@exeter.ac.uk) and Charles R. Tyler (c.r.tyler@exeter.ac.uk).

ABSTRACT:

Zinc (Zn) is an essential metal present in numerous enzymes throughout the body, playing a vital role in animal and human health. However, the increasing use of zinc oxide nanomaterials (ZnONPs) in a diverse range of products has raised concerns regarding their potential impacts on health and the environment. Despite these concerns, the toxicity of ZnONP exposure on animal health remain poorly understood. To help address this knowledge gap, we have developed a highly sensitive oxidative stress (OS) biosensor zebrafish capable of detecting cell/tissue-specific OS responses to low doses of various oxidative stressors, including Zn, in a live fish embryo.

Using live-imaging analysis with this biosensor zebrafish embryo, we discovered that the olfactory sensory neurons in the brain are especially sensitive to ZnOP exposure. Furthermore, through studies monitoring neutrophil migration and neuronal activation in the embryonic brain and via behaviour analysis, we have found that sub-lethal doses of ZnONPs (ranging from 0.033 to 1 mg/L nominal concentrations), which had no visible effect on embryo growth or morphology, cause significant localised inflammation, disrupting the neurophysiology of olfactory brain tissues and ultimately impaired olfaction-mediated behaviour. Collectively, these findings establish a potent and important effect mechanism for ZnONP toxicity, indicating the olfactory sensory system as the primary target for ZnONPs as environmental toxicant in aquatic environments. Our result also highlights that even low doses of ZnONPs can have detrimental effects on the olfactory sensory system, surpassing previous expectations. The importance of olfaction in environment sensing, sex behaviours and overall fitness across species raises concerns about the potential impact of ZnONPs on olfaction-mediated brain function and behaviour in animals and humans.

Our study emphasises the need for greater consideration of the potential risks associated with these nanomaterials.

KEYWORDS:

Nano-metal pollution, Oxidative Stress, Biosensor transgenic zebrafish, Developmental Neurotoxicity, Adverse Outcome Pathway (AOP).

Graphic Abstract

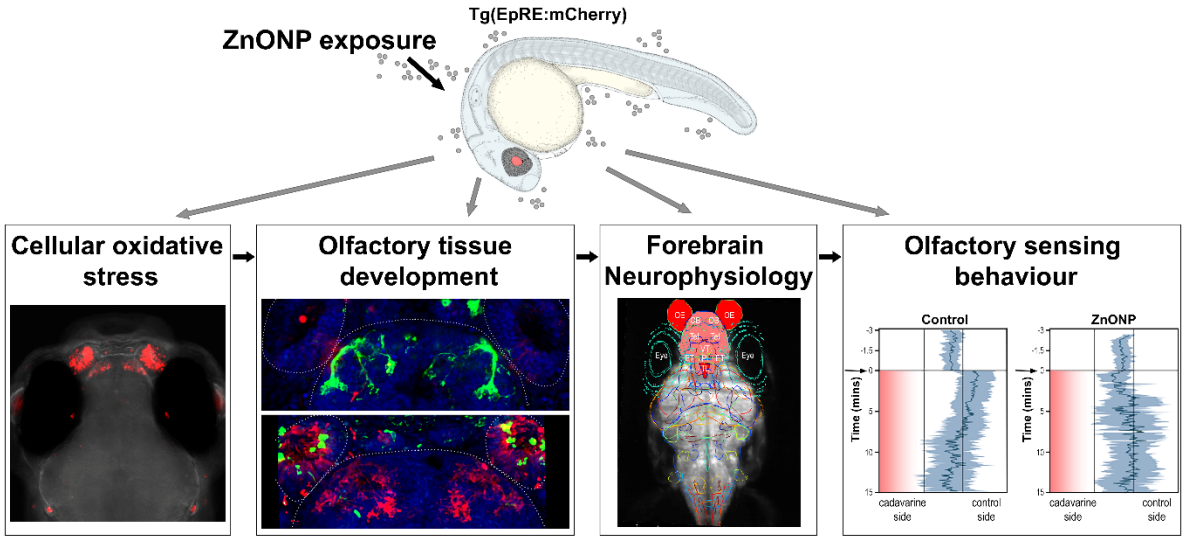

Introduction

Zinc (Zn) is an essential metal required for the health of animals and humans. It exists in numerous enzymes and proteins present across various tissues in the body, serving integral catalytic and structural functions. The cellular Zn levels are tightly controlled by the activity of different Zn transporters, ensuring proper Zn homeostasis (Haraet al. 2017; Plumet al. 2010).

Zinc oxide nanoparticles (ZnONPs) are among the most highly produced engineered metal oxide nanomaterials with an estimated annual global manufacture of 8,000 tons (Schulteet al. 2019). With their many beneficial physicochemical properties, including strong absorption of UV light, anti-bacterial/anti-fungal/anti-cancer actions and catalytic function, they are used in a very wide range of products, including in pharmaceuticals, biomedical products, cosmetics, sunscreen/UV protection, food additives, and industrial products (Sirelkhatimet al. 2015; Vimercatiet al. 2020). ZnONPs are also used as a source for micronutrients in crop fertilisers and animal foods (Radiet al. 2021; Singhet al. 2021) as Zn is essential for various physiological processes. The widespread and expanding production and use of ZnONPs, however, has also raised concerns about their potential health and environmental risks through the exposure to workers, consumers and wildlife (Adamcakova-Doddet al. 2014; Bonfantiet al. 2015; Brunet al. 2014; Jacobsenet al. 2015; Monséet al. 2018; Schulteet al. 2019; Vimercatiet al. 2020; Yanget al. 2021; Zhaoet al. 2013).

Many *in vitro* and animal model studies have shown that oxidative stress (OS) responses are one of the most likely biological mechanisms underlying the toxicity of metal-based nanomaterials, including for ZnONPs. In cell-based *in vitro* systems, exposure to ZnONPs has been shown to cause acute/chronic inflammation, damage proteins, lipids and/or nucleic acids, and induce apoptosis due to the production of excess reactive oxygen species (ROS) (Adamcakova-Doddet al. 2014;

Huanget al. 2010; Jacobsenet al. 2015; Saptarshiet al. 2015; Sharmaet al. 2012; Xiaet al. 2008). Co-treatment with the antioxidant, N-acetyl-cysteine (NAC), inhibits ZnONP-induced cytotoxicity, anti-oxidant gene induction, and pro-inflammatory cytokine release (Huanget al. 2010; Saptarshiet al. 2015; Sharmaet al. 2012), further evidencing the role of OS in ZnONP toxicity. In zebrafish embryo-larvae, ZnONP exposure induces ROS generation, activates antioxidant genes, and triggers apoptotic enzyme activation. At higher concentrations, it causes delayed hatching, embryonic malformation, and increased lethality (*e.g.* Lethal Concentration 50% (LC_{50}) = 60 mg/L) (Zhaoet al. 2016; Zhaoet al. 2013). In rodent models, ZnONP exposure via inhalation or intranasal instillation causes OS-induced pulmonary toxicities (inflammation/fibrosis) as well as neurotoxicities (cortical damage, altered neurotransmission, cognitive behavior disruption) (Adamcakova-Doddet al. 2014; Jacobsenet al. 2015; Saptarshiet al. 2015). These data strongly evidence that ZnONP exposure can disrupt normal animal development and physiology through the induction of OS. However, little is known about the tissue-specific oxidative sensitivities to ZnONP exposure, dose thresholds for ZnONP-induced OS responses, and their associated physiological and behavioural consequences, especially at environmentally relevant exposures. Such information is needed to understand more fully the potential hazards of ZnONPs in animals, including humans, and to help establish biomarkers and endpoints suitable for a more accurate evaluation of ZnONP (and other nanomaterials)-induced toxicities.

The zebrafish embryo has become an important vertebrate experimental model for (eco)toxicological assessments (Takesonoet al. 2022a). It is particularly useful for monitoring the effect(s) of environmental pollutants on the development and physiology in the embryo-larvae, due to their transparency and rapid development. Well-established gene knock-out and

transgenic technology in the zebrafish has also greatly facilitated the examination of how pollutant exposure affects specific gene function and signaling. In addition to these technical advantages, the fundamental stages of organogenesis in the zebrafish are completed within five days post fertilisation (dpf) before it is categorised as "regulated animal" under UK home office guidance (Office) as well as EU Directive 2010/63/EU (Strähleet al. 2012). Thus, the use of the zebrafish embryo for animal testing and scientific research complies favourably with the requirement for Replacement, Reduction, and Refinement of the use of animals in research (the 3Rs).

We have previously established an OS biosensor transgenic zebrafish model, tg(*electrophile response element (EpRE):mCherry*), that allows visualisation of cell-tissue-specific gene transcription in response to oxidative stress across the whole body of developing zebrafish embryos (Mourabitet al. 2019). This biosensor line utilises the Nrf2/Keap1-mediated RedOx system, where ROS triggers Nrf2 activation through Keap1 release, which in turn translocates to the nucleus and activates the *EpRE* in the genome to induce the expression of cytoprotective genes (Kobayashi and Yamamoto 2006). Combined with non-invasive imaging methods, our *EpRE:mCherry* model shows a high signal-to-noise sensitivity for a wide range of OS-inducing materials, spanning metals to pharmaceuticals, and is particularly useful for quantifying a stressor-dependent and tissue-specific OS response (Mourabitet al. 2019).

In this paper, we set out to identify the target cells/tissues and olfactory mediated consequences of early-life exposure to ZnONP, employing the tg(*EpRE:mCherry*) zebrafish model in combination with imaging methods. For this work we employed ZnONP concentrations that occur in polluted

natural environments (i.e. 33 μg/L) and a higher (but non toxic) level to help illustrate the effects mechanisms on olfactory development and function via the imaging work.

Results

Characterisation of OS-responding target cells/tissues to acute exposure of ZnONPs in OS biosensor zebrafish embryos.

To identify spatiotemporal OS responses for exposure to ZnONPs, the embryos of an OS biosensor transgenic zebrafish model, Tg(*EpRE:mCherry*), were exposed to ZnONPs (NM110, JRC) under a static exposure condition (detailed in Materials and Methods).

To verify the particle exposure conditions, the dosimetry of ZnONP and $ZnSO_4 \cdot 7H_2O$ (dissolved metal control) in the zebrafish exposure media (the egg water) were characterized. We verified that the exposure conditions used were consistent throughout the experimental periods (Suppl. Info. and Fig. S1). We also confirmed that the uptake of Zn in the exposed embryo-larvae was dose-dependent (see Suppl. Info. and Fig. S1D).

In the control group, *EpRE:mCherry* embryo-larvae generally showed minimal basal mCherry expression except for the somewhat higher basal mCherry expression in the eye lens (Fig 1. Ai-ii, Fig.S2A and S2B). With ZnONP exposure, however, we observed an intense induction of OS responses (mCherry expression) specifically in the OE and OB, two primary brain tissues involved in olfaction (Fig. 1Aiii, indicated with a white dotted square). These unique OS responses occur in a subset of OSNs, that originate from the OE and project to the OB. We also observed a relatively weaker mCherry expression in ganglions of the peripheral sensory system in ZnONP exposed embryo-larvae (Fig. 1Aiii, white arrows and Fig. S2A and S2B), suggesting ZnONPs also induce OS responses in mechanosensory cells. In addition, ZnONP exposure caused OS responses in a specific type of skin epithelial cells called ionocytes (Fig. S2A and S2B and Takesono et al. in

preparation). The OE and OB, however, were the two distinctive tissues in the brain showing ZnONP-induced OS responses.

We found that the OS responses in OSNs were detectable from exposure concentrations of 33 μg/L (≈ 405.3 nM, nominal) (Fig. 1C, indicated with white arrows) being increased in a dose-dependent manner (Fig. 1D-F, white arrows; Fig. 1J). Dissolution analysis revealed that ZnONPs dissolved in the egg water over time, with 78.2 ± 3.7% dissolution at 72h after the initiation of the incubation (Fig. S1E). These data strongly suggest that most (almost 80%) of ZnONPs were dissolved releasing Zn ions into the media during the exposure period. Indeed, we found that dissolved Zn (as $ZnSO_4 \cdot 7H_2O$) equally induced the OS response in OSNs (Fig. 1G-I). The dose-response curves of ZnONP and $ZnSO_4 \cdot 7H_2O$ were similar when the molar concentrations were compared (Fig 1J; this is a non-linear curve fit using GraphPad Prizm version 9.3.1, and involving five independent experiments for ZnONPs and two independent experiments for $ZnSO_4 \cdot 7H_2O$, with 8 replicates for each condition in each experiment), supporting the hypothesis that Zn ion is the major cause of the OSN specific OS response. Of note, no significant effects were seen on hatching rate at 72 hpf (Fig. S2C), lethality (Fig. S2D) or on embryo growth at 96 hpf (Fig S2E), regardless of the dose of ZnONP or $ZnSO_4 \cdot 7H_2O$ used in this study. The mean effective concentration (EC_{50}) for the ZnONP-induced OS response in *EpRE:mCherry* embryo-larvae was calculated as 179 μg/L (= 2.2 μM), which is approximately 45 times lower than the LC_{50} for ZnONP cytotoxicity in PMA-differentiated THP-1 macrophage cells (LC_{50} = 8.1 μg/ml) (Safaret al. 2019) and 200-335 times lower than the 96h LC_{50} for zebrafish embryos (LC_{50} = 35.88 mg/L – 60 mg/L) (Azevedoet al. 2016; Duet al. 2017). Using the *EpRE:mCherry* model our data indicate that live fish embryo-larvae show remarkable sensitivity to ZnONP-induced OS responses, even at doses

166 relevant to those measured in some polluted surface waters, without visible effects on embryo
167 development or morphology (discussed in "**Wider implications of ZnONP exposure on olfaction"**
168 section).
169
170 **ZnONP exposure affects olfactory development.**
171 To confirm the cell types responding to ZnONP exposure, ZnONP-exposed *EpRE:mCherry* embryo-
172 larvae were co-stained with anti-keyhole limpet hemocyanin (KLH) antibody, a marker for OSNs,
173 and with anti-mCherry antibody for OS responding cells. In control, the termini of KLH positive
174 OSNs form spherical clusters in the OB, which are synaptic neuropils called olfactory glomeruli
175 (Fig. 2Ai, mediodorsal glomeruli, mdGs; Fig. 2Aii, dorsolateral glomerulous, dlG and Fig. 2E). In
176 vertebrates, OSNs that express one type of olfactory receptor innervate a single glomerulus. The
177 excitability patterns in these olfactory glomeruli play a crucial role in odour sensing, forming a
178 topologically distinct representation known as the odour sensory map (Miyasakaet al. 2013). We
179 found that ZnONP exposure induced mCherry expression in the somata of OSNs in the OE (Fig.
180 2B and 2C) as well as in their projections extending to olfactory glomeruli (Fig. 2Bi-ii and 2Ci-ii).
181 Dissolved Zn also triggered OS responses in OSNs (Fig. 2D). In the embryo-larvae exposed to
182 ZnONPs and dissolved Zn, the axonal termini of OSNs in olfactory glomeruli exhibited a loss of
183 KLH expression and instead showed mCherry expression. This indicates the activation of OS-
184 mediated transcription in those regions, accompanied by morphological distortions (Fig. 2Ai-ii vs
185 2Bi-ii, 2Ci-ii and 2Di-ii; Fig. 2E vs. 2F). These data suggest that ZnONP exposure specifically
186 induced OS-mediated apoptosis in OSNs, resulting in the defasciculation of the axonal bundle of
187 the OSNs.

188 To further characterise the cell types of the OSNs, ZnONP-exposed *EpRE:mCherry* embryo-larvae
189 were stained with an anti-calretinin antibody, which is a marker for microvillous OSNs in
190 embryonic zebrafish (Koideet al. 2009). In ZnONP-exposed samples, calretinin-positive
191 microvillous OSNs maintained a typical spherical glomerular structure with no mCherry
192 expression. Notably, other OSNs expressing mCherry were present in the same olfactory brain
193 regions of the same embryo (Fig. 3A vs. 3B). The optical section images confirmed that the
194 majority of microvillous OSNs did not induce OS response even at a high concentration of ZnONP
195 exposure (1 mg/L). The expression of mCherry and calretinin thus showed a mutually exclusive
196 pattern in both cell bodies and glomerular innervations (Fig. 3Ci-iii). These data suggest that the
197 sensitivity to ZnONP differs among different types of OSNs, with KLH-positive/calretinin negative
198 OSNs (likely ciliated OSNs (Koideet al. 2009)) being more severely affected compared to
199 calretinin-positive microvillous OSNs. In addition, ZnONP exposure in the embro-larvae led to a
200 reduction in the size of the OE rosette area (Fig. 3D, * $p<0.05$, by t-test, GraphPad Prizm version
201 9.3.1, n=7), without affecting other brain regions (Fig. 3E and 3F, ns (not significant) by ANOVA
202 with Sidak's post hoc test, GraphPad Prizm version 9.3.1, n=7). These findings are consistent with
203 the observation that OS responses were exclusive to OSNs in the brain of ZnONP-exposed animals
204 (Fig. S2A).
205
206 **ZnONP exposure induces a local inflammation around the OS responding olfactory tissues.**
207 OS responses induce ROS, which subsequently triggers the progression of inflammation (Mittalet
208 al. 2014). During the initial phase of acute inflammation in zebrafish (within 30 min after an
209 injury), neutrophils are recruited to the site of the injury by sensing the ROS gradient (i.e., H_2O_2)

(Niethammeret al. 2009; Yooet al. 2011). To examine whether the ZnONP-induced OS response in OSNs caused acute inflammation, we developed and applied a double transgenic zebrafish embryo carrying both *EpRE:mCherry* and *mpx:GFP* (neutrophil-specific) reporter genes, which allows for the simultaneous monitoring of OS-responding OSNs (mCherry) and neutrophils (GFP). With this line, we investigated whether ZnONP exposure affects the migratory behaviour of neutrophils, that reflects their infiltration and activation status upon a local inflammation. We also examined the spatial relationship between OS-responding OSNs and neutrophils in the olfactory tissues. We found that the number of neutrophils in the head/brain regions was significantly increased by ZnONP exposure (Fig. 4A, left-end column). This increase was dose-dependent and particularly evident in the anterior part of the brain, in the area in close proximity to the OS-responding OSNs (Fig. 4Bi and Fig. 4Ci; details in Materials and Methods). Applying trajectory analyses for migrating neutrophils, we found that many neutrophils were retained around OS-responding OSNs in ZnONP-exposed embryo-larvae: in the anterior head/brain region, total distance moved (Fig. 4Bii), displacement (start-end distance: Fig. 4Biii) and migration speed (Fig. 4Biv) of neutrophils were consistently reduced by ZnONP exposure in a dose-dependent manner. In contrast, in the mid-region of the head, which is distant to the OS-responding OSNs, no change in the migratory behaviour of neutrophils was observed except for a reduction in the migration speed in the animals exposed to I mg/L ZnONPs (Fig 4Cii-iv). These data indicate that neutrophils can detect the location of the OS-responding OSNs in ZnONP-exposed animals and likely contribute to the acute inflammation in the local microenvironment.

ZnONP exposure alters the intrinsic/spontaneous neuronal activity in the olfactory brain regions in the embryonic brain.

Next we explored the neurophysiological consequence of the ZnONP toxicity in relation to OSN-specific OS responses. For this, we employed the live calcium imaging analysis using *elavl3:GCaMP6s* transgenic zebrafish model that has been established previously in our laboratory (details in (Takesonoet al. 2022b; Winteret al. 2017)). Using this system, a full brain volume of live imaging of the calcium indicator, GCaMP6s, was obtained and the region of interest (ROI)-specific neuronal activity data was subsequently extracted. With this, we found that ZnONP-exposure led to a significant increase in intrinsic GCaMP signals primarily in the anterior forebrain regions (group I in Fig. 5B; details in Materials and Methods). This increase was particularly evident in the OE and OB, the specific olfactory brain tissues exhibited pronounced OS responses to ZnONPs. Similar effects were observed in some surrounding ROIs in the diencephalon (group II) and in a specific brain region in the midbrain (mesencephalon)(group III). ZnONP effects on neurophysiology of wider ROIs may be due to the functional interconnectivity between these olfactory tissues and the other brain regions. Collectively, our data indicate that ZnONP exposure alters intrinsic neuronal activity in a region-specific manner, correlating with its effects on region-specific OS responses, alterations in OSN development, and the resulting local inflammation.

ZnONP exposure impairs olfaction-mediated avoidance behaviour.

Finally, we addressed whether this OSN-specific toxicity of ZnONP could affect olfaction-mediated behaviour. To do so, we examined the odour-evoked avoidance behaviour using a

death-associated odour, cadavarine, as an aversive olfactory cue (Takesonoet al. 2022b). A group of 10 embryo/larvae were placed in the middle area of a test chamber which was partitioned into three areas by removable dividers (Fig 6A). The movement of the test individuals was video-recorded and automatically tracked using the multiple object tracking system in idTracker software (Pérez-Escuderoet al. 2014). During the acclimation period (before applying cadavarine), both control and ZnONP-exposed embryo-larvae showed no significant difference in swimming capability (total distance travelled during the last 5 min of acclimation: 98.03 ± 5.40 mm for control vs. 85.33 ± 7.64 mm for ZnONP-exposed group)(Fig. 6C, acclimation, left). With cadavarine administration following divider removal, the test animals were subsequently exposed to the cadavarine gradient. We found that control fish responded to cadavarine by avoiding the side of the tank with a higher cadavarine gradient (Fig. 6B, control, left), travelling greater distances (Fig. 6C, cadavarine, right), and spending more time at the opposite end of the chamber (Fig. 6D). In contrast, ZnONP-exposed fish showed reduced responsiveness to cadavarine, remaining around the centre of the chamber where the fish were originally placed (Fig. 6E). Thus, the total distance travelled during cadavarine exposed period (Fig. 6C, cadavarine, right: 866 ± 98.06 mm for control vs. 390 ± 42.38 mm for ZnONP groups) and the centroid distance from the cadavarine administrated site over the acquisition time (avoidance index) were significantly reduced in ZnONP-exposed groups (Fig. 6F). These data indicate that ZnONP exposure impairs olfaction-mediated avoidance behaviour in zebrafish embryos-larvae, reflecting specific OS responses in OSNs and resultant defects in olfactory development and function.

Discussion

ZnONP exposure induces the OSN-specific OS response, resulting in adverse effects on olfactory tissue development, neurophysiology and behaviour.

We have shown previously that our tg(*EpRE:mCherry*) model can effectively identify distinct tissue-specific OS responses to a diverse range of chemical and other stressors. Illustrating this, acetaminophen (paracetamol) triggers OS responses in the liver, cisplatin in hair cells, phenylhydrazine in red blood cells and Cu^{2+} ions in skin ionocytes (Mourabit M. 2019). Thus, our OS biosensor zebrafish model discerns chemical-specific target cells/tissues, reflecting its specificity in responding cell types and its mode of action (Mourabit M. 2019). Using the OS biosensor zebrafish model, here we show that ZnONP-exposure causes olfactory tissue-specific developmental neurotoxicity via the induction of OS response in the OSNs. This neurotoxicity was induced by sub-lethal exposure concentrations of ZnONPs, with which no effect on overall morphological development, hatching rate, embryo size (growth) or survival rate was observed in zebrafish embryo-larvae. Using whole-mount immunohistochemistry and other transgenic zebrafish models, we showed that ZnONP-exposure leads to defects in OSN development and olfactory tissue-specific inflammation, and subsequently alters the neurophysiology in the forebrain regions and disrupts olfaction-mediated behaviour in the zebrafish embryo-larvae. In light of this, our data unveil OSNs as a primary target tissue for ZnONP neurotoxicity, and illustrate that sub-lethal exposure concentrations of ZnONP impact neurodevelopment, physiology, and behaviour in live fish embryos. Whether this effect may occur for other metal based nanomaterials has yet to be explored fully, but for studies on Cu^{2+} exposure (0.6-6.5 μg/L) in tg(*EpRE:mCherry*) embryos we

have not found evoked OS responses in OSNs but rather induce marked responses for this metal in skin ionocytes (Mourabit M. 2019).

The olfactory epithelium: the primary uptake site of ZnONPs in the brain.

In our OS biosensor model, ZnONP exposure induced OS response exclusively in a few specific cell types, including OSNs in the brain (this study) and skin and gill epithelial cells (Fig. S2A-B, Takesono et al. in preparation). These cells are commonly in direct contact with the aquatic environment and therefore likely to be especially vulnerable to chemical exposures. From this viewpoint, the OE is likely to be the first entry site for ZnONPs into the brain of fish embryo. This is supported by our data that intense OS responses (indicated by mCherry expression) were seen only in the cell bodies of OSNs in the OE and their axons in the OB, while no mCherry expression was observed in other cells in the brain (Fig. 1Aiii, Fig. 2A and 2C). These findings suggest that ZnONP-induced OS responses occur along peripheral (the OE) – central (the OB) axis of OSNs in the zebrafish embryo-larvae.

Under our exposure conditions, it appears that the dissolved Zn ion, rather than the particulate ZnONP, is responsible for the OS responses in OSNs. This is supported by the fact that the by 96 hours of exposure the majority (over 80%) of ZnONPs had dissolved in the exposure media (Fig. 1SE) and given the approximate EC_{50} values for the OS response for both ZnONP and Zn ion exposures (Fig. 1J). The dissolved Zn ion from ZnONPs is likely taken up into the cytoplasm of OSNs by specific isotypes of Zn transporters expressed in their transmembrane. In zebrafish, there are total 18 Zn transporters which are involved in either Zn influx or efflux (Feeneyet al. 2005).

Zn plays a crucial role in the brain, regulating transcription during neurogenesis and differentiation, neurotransmission and neuronal apoptosis following injury or ischemia (Fredericksonet al. 2005; Plumet al. 2010). Previous studies have shown that intracellular concentrations of Zn are particularly high in specific brain regions in rodents, including the olfactory bulb. Zinc autometallography (AMG) and immunostaining of Zn transporters, such as ZnT1 and ZnT3 involved in Zn efflux, have revealed the complementary enrichment of Zn ion and Zn transporters in the outer part of each olfactory glomerulous which consists of OSN termini and dendrites from mitral cells and periglomerular cells (Joet al. 2000; Sekleret al. 2002). These findings suggest specific roles of Zn in the development and function of olfactory glomeruli. OSNs may possess an inherent ability to efficiently incorporate Zn ions into their cytosol, which could lead to disruptions in Zn homeostasis upon ZnONP exposure and heightened susceptibility to ZnONP toxicity. The distinct OS responses in OSNs may be due to the specific expression of Zn transporters within these cells. Further study into the specific expression patterns and roles of these transporters in OSNs in zebrafish embryo-larvae would enhance our understanding of the potential mechanisms involved in Zn uptake and efflux related to ZnONP toxicity.

Wider implications of ZnONP exposure on olfaction

The concentration range of ZnONP used in this study, with nominal concentrations between 33 μg/L and 1 mg/L and measured concentrations between 54.18±16.25 and 762±18.18 μg/L (Fig.S1A), is considerably lower than those reported in previous studies on ZnONP toxicity in zebrafish embryo-larvae (Azevedoet al. 2016; Duet al. 2017) and with relevance to environmental concentrations of Zn. Our dissolution analysis showed that most of ZnONP (about 80%) was

dissolved in the water by 72 hours of the exposure (Fig. S1E), and the toxicities of ZnONP and Zn ion for OSNs did not appear to differ (Fig. 1 and Fig. 2). Thus, the toxic effects on OSN are most likely to be due to Zn ions rather than ZnONP particles themselves.

Zn is a relatively abundant metal, and ZnONP may contribute considerably to the bioavailable source in the environment (Larneret al. 2012). The environmental quality standard (EQS) values for Zn vary globally (Vorkamp 2016), with EQS values ranging from 10.9 μg /L In UK freshwaters (Affairs. 2014) to 30 μg /L in Japan (Naitoet al. 2010; Shikazonoet al. 2008). In Europe the EQS for ZnONPs has been estimated at 10 μg/L, calculated based on a probabilistic material flow modelling analysis (Gottschalket al. 2009). Importantly, surface water monitoring data have shown Zn concentrations exceeding EQS levels in various locations, most notably around industrial areas and mining sites. In the case of the latter Zn has been measured in excess of 445 μg/L (e.g. in the River Teign, UK (Jordanet al. 2020) and Shiine river, Japan (Shikazonoet al. 2008)) and up to 935 μg/L in the River Hayle, UK (Minghettiet al. 2014). Surface water monitoring data for Zn in Japan between 1991 to 2002 across 3347 sites found that approximately 20% of the test sites exceeded the national EQS (30 μg/L), including near the municipal wastewater treatment plants for household wastes (concentrations of Zn ranged between non detectable to 2.9 mg/L) (Naitoet al. 2010). Thus, the ZnONP exposure concentrations in our study can be considered as within the environmental concentration range, making our findings on ZnONP-induced olfactory-disruption relevant to freshwater bodies worldwide.

Olfaction is essential for various animal behaviours such as foraging, kin-recognition, predator avoidance, mating, and eco-location (Wyatt 2003). Olfaction dysfunction may also affect the

social and sex behaviours and fitness of the animals. Importantly, the principal mechanisms underlying the organisation of olfactory system and odour processing are highly conserved across diverse phyla and indeed most animal species, including worms, insects, fish, rodents and humans (Ache and Young 2005). Thus, neurotoxicity of ZnONP reported in this study suggests a potential global risk to animal and even human health. To what extent the ZnONP-mediated developmental neurotoxicity in OSNs affects odour sensing in later-life and/or the adulthood remain unknown and warrants further investigation.

Conclusions

Using an OS biosensor zebrafish model, we have discovered a unique neurotoxic effect of ZnONPs on OSNs during developmental stage of zebrafish embryo-larvae. This specific OS response in OSNs leads to defects in OSN development and localised inflammation in olfactory tissues, and disruptions in neurophysiology and olfaction-mediated behaviour. Remarkably, these OS-mediated defects in olfactory sensory system occur even at low exposure concentrations of ZnONP, without any visible effects on embryo growth or morphology, highlighting their direct relevance as a primary mechanism of ZnONP toxicity in the environment. Our study emphasises the importance of research into olfactory sensing systems of fish (and other organisms) when assessing the potential hazards associated with exposures to metal based nanomaterials and potentially other types of toxicants.

Materials and Methods

383

384 **Experimental zebrafish lines and fish husbandry**

385 The oxidative stress biosensor transgenic zebrafish line, Tg(*EpRE:mCherry*), used in this study has
386 been described previously in (Mourabitet al. 2019). The double transgenic of EpRE:mCherry and
387 mpx:GFP (neutrophils line; generously provided by Stephen A. Renshaw, University of Sheffield),
388 Tg(*EpRE:mCherry; mpx:GFP*), were produced from a pair-cross of homozygous parents of each
389 TG fish line (detailed in SI, Suppl. Materials and Methods). The *elavl3(huC):GCaMP6s* transgenic
390 zebrafish line, Tg(*elavl3:GCaMP6s*), has also been described previously in (Takesonoet al. 2022b;
391 Winteret al. 2021; Winteret al. 2017) and was originally supplied by Misha B. Ahrens (Janelia
392 Research Campus, Howard Hughes Medical Institute, Ashburn, Virginia, USA). Adult zebrafish
393 were maintained in flow through aquaria in the aquatic resource centre at the University of
394 Exeter on a g 14/10 light/dark cycle at 28 ± 1 °C. All procedures for fish husbandry and the
395 experiments conducted with zebrafish were in accordance with U.K. Home Office regulations for
396 the use of Animals in Scientific Procedures Act (1986) and followed local ethical review guidelines
397 for ensuring their humane treatment.

398

399 **ZnONP and $ZnSO_4 \cdot 7H_2O$ exposure**

400 A stock ZnONP (NM110, JRC) suspension was made up at a concentration of 2.56 mg/ml in MilliQ
401 water was prepared following the NANoReg_Ecotox dispersion protocol version 6 (Booth 2015)
402 using a probe-sonicator (Cole-parmer, CPX 130 ultrasonic processor). For this, the amplitude and
403 duration of the sonication collectively delivered a total acoustic power (Pac) of 7.35±0.05 Watts.
404 The stock ZnONP suspension was then left for overnight at room temperature to achieve

suspension equilibrium. Prior to the initiation of the embryo exposures, the ZnONP stock suspension was re-suspended via a brief (30 sec) water-bath sonication and the solution was then used immediately to make up a series of working exposure dilutions in the zebrafish embryos exposure media (egg water; 60 mg/L artificial sea salt, The Tropical Marine Centre). EpRE:mCherry embryos were collected by natural spawning, cleaned and cultured in the egg water at 28°C until 24 hpf. Healthy 24 hpf EpRE:mCherry embryos were then exposed under static systems to freshly prepared ZnONP suspensions at concentrations of 33, 100, 330 μg/L and 1 mg/L , for 72 hours (until 96 hpf) at 28°C. This was carried out in 24 well plates at a density of 5 embryos/2ml media/well. Further sets of EpRE:mCherry embryos were exposed to $ZnSO_4 \cdot 7H_2O$ (dissolved Zn) at water concentrations ranging between 100 μg/L and 10 mg/L under the same exposure conditions as described for ZnONP above, that lead to comparative OS responses in olfactory tissues as those induced by used ZnONP concentrations. Control EpRE:mCherry embryos were prepared by exposing to the egg water only in the same incubation conditions. All experiments were repeated at least twice and each experiment was conducted with a different batch of EpRE:mCherry embryos, freshly prepared ZnONP/Zn ion suspension, and with 8 replicates per treatment condition.

Imaging and quantification of tissue specific OS responses

For imaging of tissue specific OS responses, 96 hpf control, ZnONP or dissolved Zn exposed EpRE:mCherry embryos were anaesthetised with 0.03% MS222 in egg water and quickly mounted in 0.7% low melting point agarose in a 35 mm diameter glass-bottom dish (MatTek) for microscopic observation. For dose-response analyses, epifluorescent images of oxidative stress

responses (read-out as tissue specific mCherry expressions) in control and ZnONP and dissolved Zn exposed embryos were acquired using fluorescence light microscopy (Zeiss observer Z1; Zeiss, Cambridge, UK) with a metal halide fluorescent light source (HXP 120C, Zeiss, Cambridge, UK) and a 20x objective lens. The imaging parameters (e.g. the exposure time and intensity of the fluorescent light, z-step size) were optimised to avoid the saturation of mCherry signal in the embryo-larvae samples at the highest dose of ZnONP or dissolved Zn exposure and to ensure inclusion of all signals in the OE and the OB, and the imaging parameters were kept consistent for each experiment. The acquired images were processed using Fiji with set parameters for brightness/contrast adjustment and background subtraction. To quantify OS responses in the OE, the average intensity projection image of each sample was obtained and the mean grey value of mCherry signal within the OE was measured. The OE region was identified by tracing the outline of the olfactory rosette in the DIC image. The background grey value in the equivalent area size of non-fluorescent brain region was subtracted from the raw grey value of the mCherry signals in the OE for each sample. Data (Fig. 1J) are shown as Log (OS response = grey vale) plotted against log (M) of ZnONP or $ZnSO_4 \cdot 7H_2O$ concentration, and curve fits calculated and applied using GraphPad Prism 9.0. For representative images (Fig 1A-I), Zeiss LSM880 airyscan operated by Zen Black software was used keeping at a set (and/or optimal) z step size. mCherry Images were airy processed in Zen Black software and DIC images were processed using extended depth focus (EDF) function in Zen Blue software. Processed images were merged and further processed using Fiji with set parameters for the adjustment.

Assessment of local inflammation in live zebrafish embryos

A double transgenic of EpRE:mCherry and mpx:GFP (neutrophils), Tg(*EpRE:mCherry; mpx:GFP*), was used to observe the ZnONP-induced OS response in the OSNs and simultaneously monitor the migratory behaviour of neutrophils in the same embryo-larvae. Exposure conditions and sample preparation for live imaging are as described in "Imaging and quantification of tissue-specific OS responses" section. Live imaging of mCherry-expressing OSNs and GFP-expressing neutrophils was carried out using Zeiss 880 in fast acquisition mode with Airyscan, which achieves nine consecutive optical *z*-section images extending through the entire forebrain-midbrain regions (scan depth 120 µm, 12 µm step each) in 2.2 s, allowing tracking of migratory trajectories of neutrophils in the whole forebrain-midbrain regions. The time-lapse images were obtained every 2 minutes for 20 minutes. The acquired images were airy processed in Zen Black software and were further processed using Fiji with set parameters for the adjustment. Migratory parameters of neutrophils in the anterior brain and the mid-brain regions were analysed using Manual tracking plugging in Fiji. Data were obtained from two independent experiments, with four individual fish embryos as experimental replicates, and analysing migratory behaviour of 13-15 neutrophils per embryo. Data analyses were carried out using ANOVA with Tukey's post hoc test using GraphPad Prizm version 9.3.1.

GCaMP6s imaging

The detailed procedures for sample preparation for GCaMP6s imaging and for imaging acquisition using a custom-built LSM are described in (Takesonoet al. 2022b; Winteret al. 2017). Exposure of Tg(*elavl3:GCaMP6s*) embryo-larvae to 125, 250 µg/L ZnONP was conducted as described in the section" ZnONP and $ZnSO_4 \cdot 7H_2O$ exposure". At 96 hpf (72 h exposure), exposed

fish were pre-screened for a similar basal GCaMP expression level in the brain before LSM imaging. All experimental treatments were conducted using the same batch of embryos, and each experiment was repeated on two separate occasions, to account for possible batch-to-batch variation. Data analyses were carried out using mixed effect generalised linear model in R v. 3.2 (Team 2013). N=7-9.

Whole-mount immunohistochemistry

All whole-mount immunohistochemistry was conducted with 4% paraformaldehyde (PFA)-fixed 4 dpf EpRE:mCherry embryos that had been exposed to ZnONP or dissolved Zn or non-exposed controls, as described above. See further details in (Takesonoet al. 2022b).

Olfaction-mediated avoidance behaviour assays

EpRE:mCherry embryos were cultured with or without 1 mg/L ZnONP as described above at a density of 50-70 embryos in 75 ml of the egg water in a glass dish. Olfaction-mediated avoidance behaviour was assessed in infrared light in an enclosed box using automated video-tracking system (PGRFlyCap software) with a video camera at 20 frames per second. At 5 dpf, 10 healthy fish were placed in the middle zone in a test chamber (10.5 cm x 3.5 cm x 1.7 cm)(Fig. 5A) containing 15 ml of the egg water held in an enclosed light box with a camera attached to the top of the box. The fish in the test chamber were acclimated for 15 minutes and their movement during the last 5 minutes of the acclimation period was video-recorded to assess their migratory activity (acclimation phase). A fear-associated aversive odorant, cadavarine (20 µl of 10 mM), was subsequently administrated at the edge of either side of the arena (the side of administration

493 was alternated between trials in a semi-random manner). After a 5-minute equilibration period,
494 the dividers were removed and the movement of fish video-recorded for 10 min (test phase).
495 Acclimation and test phase videos were analysed using the multiple subject tracking system in
496 idTracker software v2.1. (Pérez-Escuderoet al. 2014). In each trial the movement of individuals
497 was analysed and extracted in the form of x-y coordinates. Using the extracted coordinates, the
498 overall distance travelled for each individual was calculated, both for the acquisition and for the
499 test phase. Individual fish that remained static for >50% of the frames analysed per trial were
500 excluded from further analysis; these were evenly distributed across experimental conditions.
501 The mean centre of mass (centroid) was calculated for each experimental group and the shift of
502 the centroid from the centre of the arena was determined as a measure of the response to the
503 cadaverine administration during the test phase.
504 The distance travelled during the acquisition phase as well as the test phase was analysed using
505 generalised linear mixed effect models in the 'lme4' v1.29 R package (Bates 2010); the full models
506 included condition (Control/ZnONP) as a fixed factor and an individual trial-level as random
507 effects. The shift of the centroid from the centre of the test arena during the test phase was also
508 analysed using a generalised linear mixed effect model using the 'lme4' R package. The full model
509 included the experimental condition (Control/ZnONP), the side of administration (Left/Right to
510 control for any bias), the standardised average of the distance moved by the group of individuals
511 (calculated separately for each treatment as a z-score); day was included as a random factor,
512 while the sequence in which the animals were tested was found not to explain any of the variance
513 and was therefore omitted. In all cases the family (the error structure, i.e. the probability
514 distribution of the errors) and link function (i.e. the function relating the mean value of y to the

515 fixed factor) were chosen for the best fitting-model. All models met their assumptions and were
516 validated through diagnostic plots. All statistical analyses were carried out in R v. 3.2 (Team
517 2013).

518 **FIGURES**

519 Figure 1

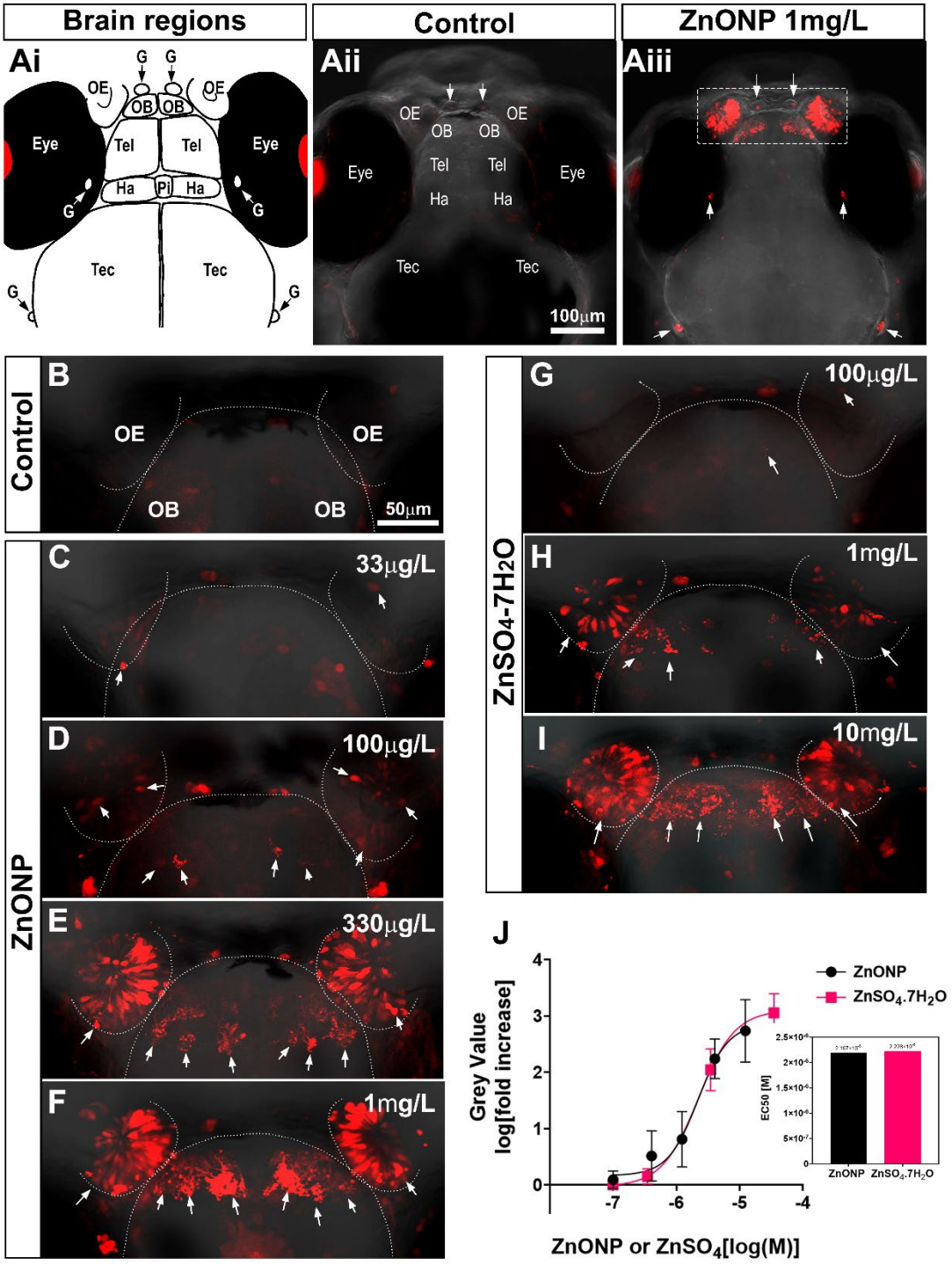

520

521 **Figure 1. ZnONP exposure specifically induces OS responses in the OE and OB.** (Ai) Forebrain -

522 and Midbrain regions in 4 dpf zebrafish embryo-larvae. OE, olfactory epithelium; OB, olfactory

bulb; Tel, telencephalon; Ha, habenula; Pi, pineal; Tec, tectum; G, ganglions; Eye. (Aii-iii) Confocal image of control (Aii) and ZnONP (1mg/L) exposed (Aiii) *EpRE:mCherry* embryo-larvae. Dotted white square in Aiii, OS responses in the OE and OB; OS responses in ganglions, white arrows. (B-I) ZnONP and dissolved Zn induce a concentration-dependent OS responses in the olfactory tissues. Control (B); ZnONP 33μg/L (C), 100μg/L (D), 330μg/L (E), 1mg/L (F); $ZnSO_4 \cdot 7H_2O$, 100μg/L (G), 1mg/L (H) and 10mg/L (I). OS responding cells, white arrows; the outlines of the OE and OB, white dotted lines. Scale bar, 50μm. (J) The dose-response curves of ZnONP (black) and $ZnSO_4 \cdot 7H_2O$ (pink) were similar when the molar concentrations were compared. The mean grey value (fluorescent intensity) ± SEM are shown as log [fold increase of grey value] in the OE. EC_{50} are shown in the inset bar graph. Non-linear curve fitting was applied to calculate EC_{50} values using GraphPad Prizm version 9.3.1. Data were derived from five independent experiments for ZnONPs and two independent experiments for $ZnSO_4 \cdot 7H_2O$, with 8 replicates for each condition per experiment.

Figure 2.

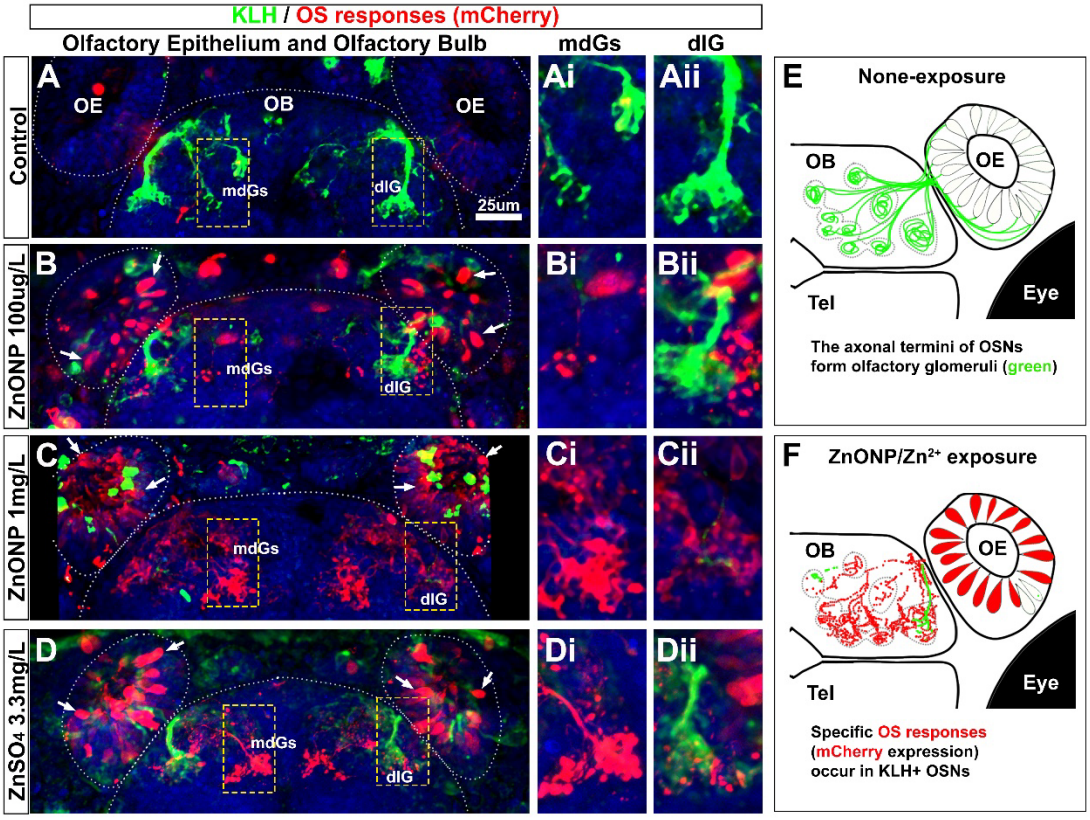

Figure 2. ZnONP exposure induces OS responses in olfactory sensory neurons. (A-D) Confocal images of key limpet haemocyanin (KLH) positive axonal projections of olfactory sensory neurons (OSNs) (green) and mCherry expressing OS responding cells (red) in the OE and OB. The nuclei staining (blue) and white dotted lines, represent the outline of the OE and OB (A-D); olfactory glomeruli, yellow dotted rectangles in A-D; mediodorsal glomeruli, mdGs (Ai-Di); dorsolateral glomerulous, dlG (Aii-Dii); the cell bodies of OS responding OSNs, white arrows (B-D). Scale bar, 25µm. (E, F) Illustrations of changes in olfactory tissues with (F) or without (E) ZnONP or dissolved Zn exposure to *EpRE:mCherry* zebrafish embryo-larvae. Control OSNs (green); OS responding OSNs (red); olfactory epitheium, OE; olfactory bulb, OB; Telencephalon, Tel.

548 Figure 3.

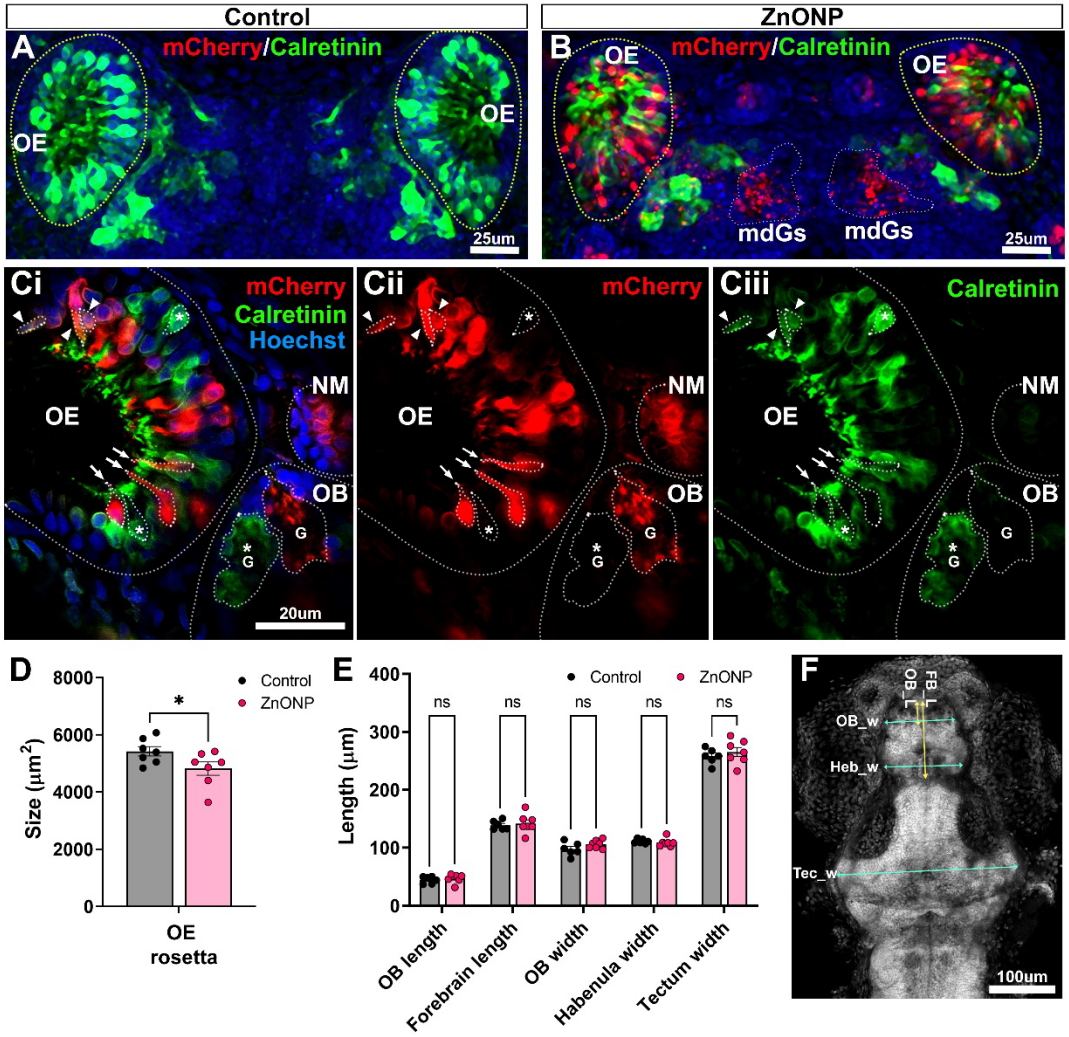

549

550 **Figure 3. ZnONP exposure primarily triggers OS responses in calretinin-negative OSNs.** (A-B)
551 Confocal images of a microvillous OSN marker, calretinin, positive OSNs (green) and mCherry
552 expressing OS responding OSNs (red) in the OE and OB: A, control; B, ZnONP (1 mg/L) exposed
553 EpRE:mCherry embryo-larvae. The outlines of the OE, yellow dotted lines; OS responding OSN
554 projections at mdGs, white dotted lines in B; the nuclei, Hoechst staining (blue). (Ci-Ciii) The
555 optical section image (0.5μm step size) of OS responding (Cii, mCherry) and calretinin expressing
556 (Ciii, green) OSNs in ZnONP (1 mg/L) exposed *EpRE:mCherry* embryo-larvae. neuromast, NM;

glomerulus, G; mCherry (red)+ OSNs, white arrows; calretinin (green)+ OSNs, white asterisks; mCherry+/calretinin+ double positive OSNs, white arrow heads; the nuclei, Hoechst staining (blue). (D) The measurement of OE rosette area size, and (E) brain region length, n=7. Mean ± SEM with individual plots shown. (F) The representative positions of the measurements used for E: the lengths, yellow both-end arrows; the widths, cyan both-end arrows. * $p<0.05$, by t-test in D; ns (not significant) by ANOVA with Sidak's post hoc test using GraphPad Prizm version 9.3.1.

564 Figure 4.

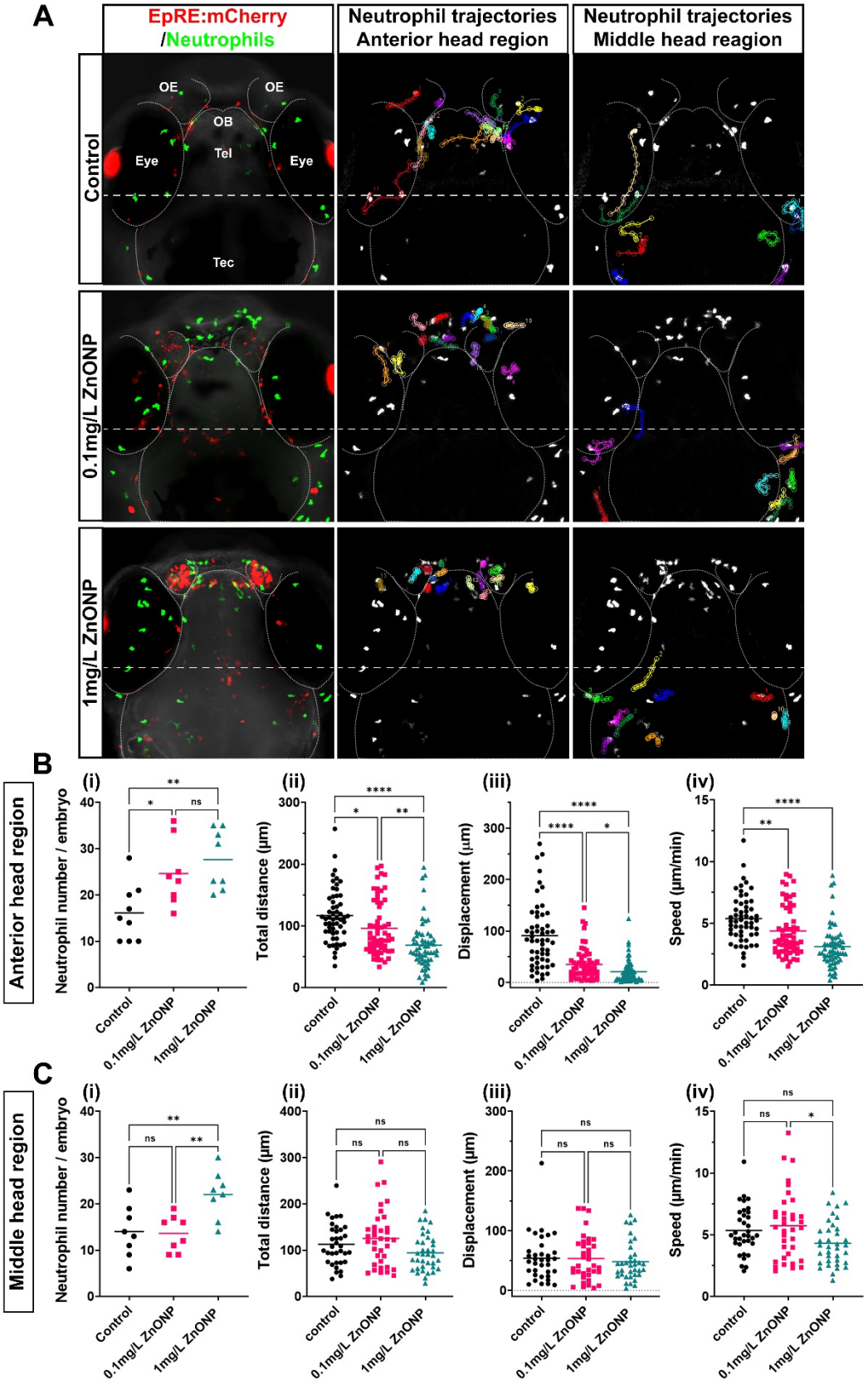
A
EpRE:mCherry
/Neutrophils
Neutrophil trajectories
Anterior head region
Neutrophil trajectories
Middle head reagion
Control
0.1mg/L ZnONP
1mg/L ZnONP
OE
OE
OB
Tel
Eye
Eye
Tec
B
Anterior head region
(i)
(ii)
(iii)
(iv)
Neutrophil number / embryo
Total distance (μm)
Displacement (μm)
Speed (μm/min)
Control
0.1mg/L ZnONP
1mg/L ZnONP
control
C
Middle head region
ns

Figure 4. ZnONP exposure induces a local inflammation in close proximity to OS responding olfactory tissues. (A) Confocal images of neutrophils (green) and mCherry expressing OS responding OSNs (red) in control (top) or 0.1 mg/L (middle) or 1 mg/L ZnONP (bottom) exposed double transgenic Tg(*EpRE:mCherry*;*mpx:GFP*) embryo-larvae. (The left panels) The merged images at the final time point of the time-lapse (20 minutes) (the middle panels); The trajectories of neutrophils in the anterior-brain region (upper half from the dotted line in the image); The trajectories of individual neutrophils, coloured lines (The right panels); The trajectories of neutrophils in mid-brain regions (lower half from the dotted line in the image). (Bi-iv and Ci-iv) Dot plots for total neutrophil numbers (Bi and Ci, n=8-9); total distance (Bii and Cii); displacement (start-end distance) (Biii-Ciii) and speed (Biv-Civ) of neutrophil migration during 20 minutes timelapse imaging are shown. The above parameters in anterior-brain region (Bi-iv); in mid-head region (Ci-iv) are shown. * $p<0.05$, ** $p<0.01$, **** $p<0.0001$ and ns (not significant) by ANOVA with Tukey's post hoc test using GraphPad Prizm version 9.3.1.

579 Figure 5.

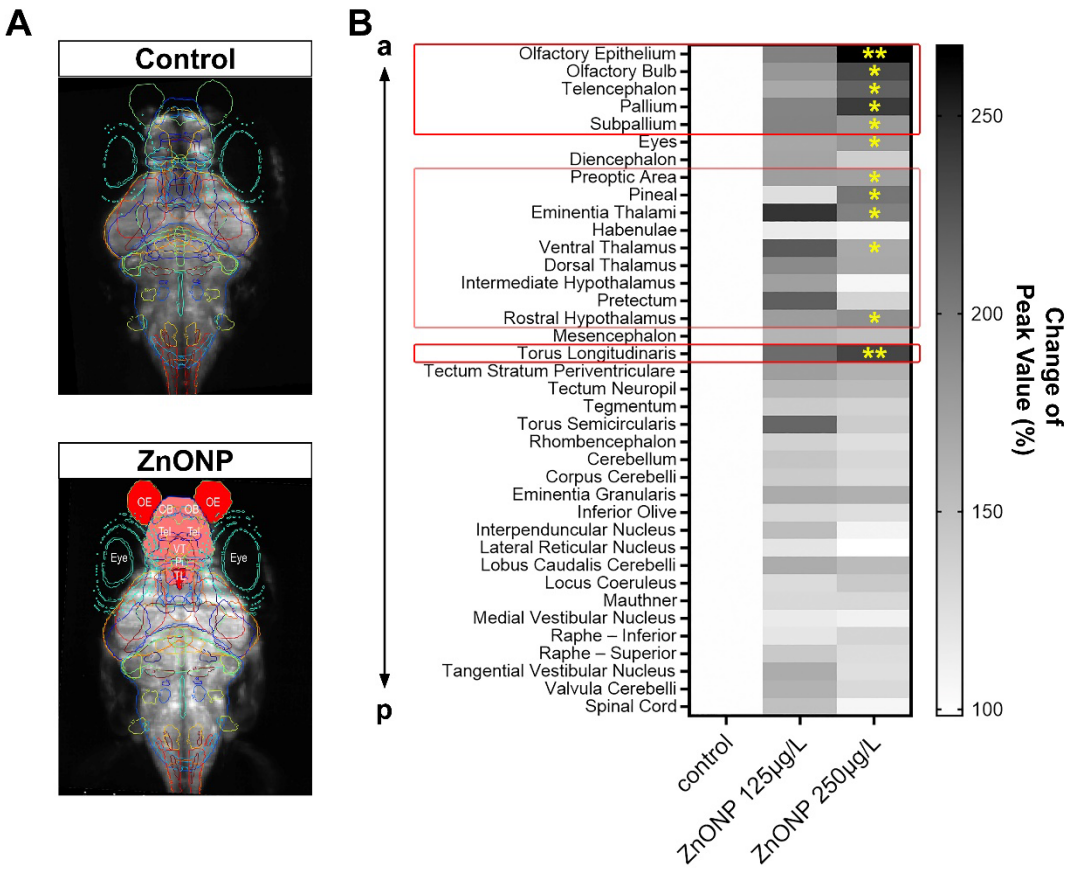

580

581 **Figure 5. ZnONP exposure alters the intrinsic neuronal activity predominantly in forebrain**
582 **regions linked with odour processing.** (A) LSM images of *elavl3:GCaMP6s* zebrafish embryo brain
583 (dorsal view) of control (top) and ZnONP (250 µg/L) exposed embryos (bottom) (see details in
584 Methods). Each coloured line in the images represents a brain region of interest (ROI). ROIs
585 whose GCaMP activity are activated by ZnONP are coloured with gadiented red (based on the
586 data in Fig.5B). Olfactory epithelia, OE; olfactory bulb, OB; Telencephalon, Tel; Ventral Tharamus,
587 VT; Pineal, Pi; Torus Longitudinalis, TL. (B) Heat map displaying changes (%) of GCaMP signals in
588 37 different brain regions. The order of ROIs represents the location of a ROI along anterior-
589 posterior (a-p) axis (top-bottom). ROIs with a significant increase in the intrinsic neuronal activity

590 are marked with red rectangles. Forebrain regions, I; mid-brain (diencephalon) regions, II; and
591 Torus Longitudinaris, III. * $p<0.05$, ** $p<0.01$ by mixed effect generalised linear model in R. N=7-
592 9.

593

Figure 6.

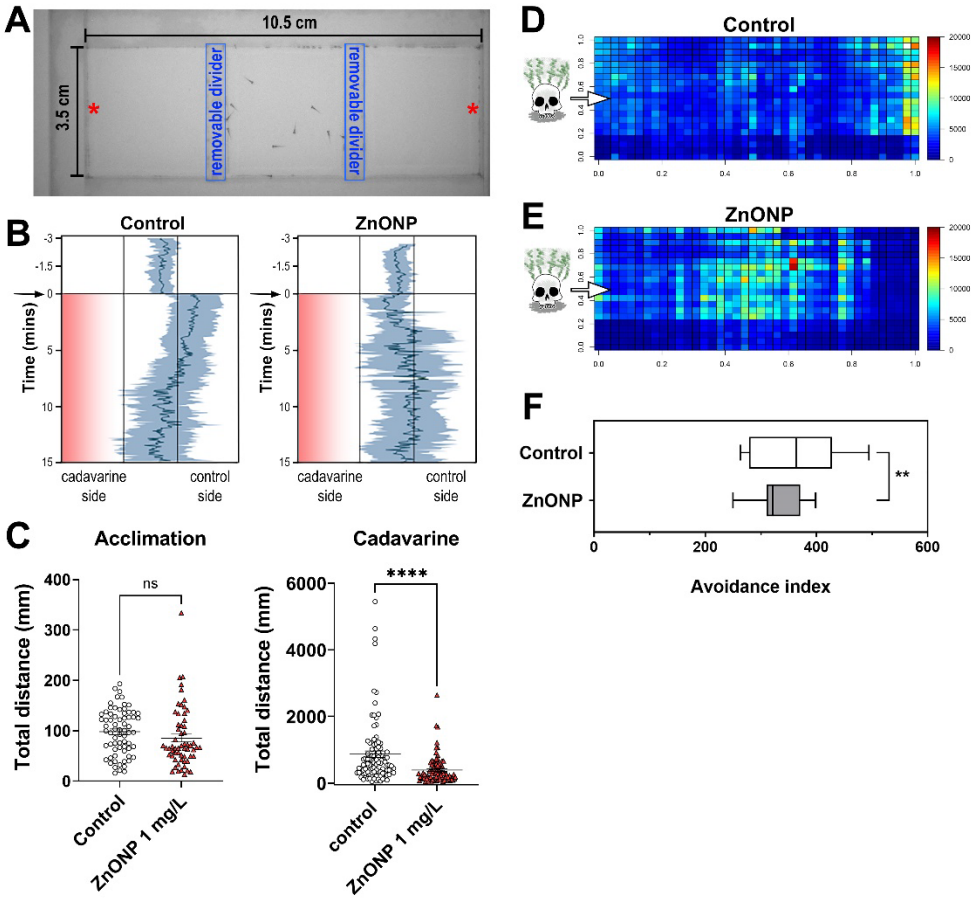

Figure 6. ZnONP exposure impairs olfaction-mediated avoidance behaviour. (A) Illustration of the experimental arena. A fear-related aversive odorant, cadavarine, was administrated at the edge of either side of the arena (red asterisks). (B) Representative data showing the mean (dark grey line) or standard deviation (shading) positions of 10 individual of control or 1 mg/L ZnONP exposed 5 dpf *EpRE:mCherry* larvae plotted along the horizontal axis of the experimental arena every two second. Cadavarine was applied at time -5 on the left edge and equilibrated for 5 min within the left compartment. The dividers were then removed at time 0 (indicated by arrows) to expose the experimental animals to the cadavarine gradient (red gradient). (C) Dot plots showing

604 total distance travelling during acclimation (left panel) or after cadavarine exposed period (right
605 panel). Data of total 60-99 fish from 6-10 groups are shown. Not significant, ns; p<0.0001, ****
606 by t-test. (D and E) Colour-coded heat maps indicating the sum of durations for the presence of
607 individual larvae in each square area. The heat maps are plotted from combined data from four
608 independent groups (each 10 fish) of control (top) and ZnONP (1 mg/L)-exposed larvae (bottom).
609 The site of cadavarine administration is indicated with while arrows on the left. (F) The box plots
610 for the means of centroid distance from the site of cadavarine administration over the 10 min
611 acquisition time are shown as “Avoidance index”. Data are from nine groups for each condition
612 including the groups with cadavarine administration at either left or right site. ** p <0.01 with
613 mixed effect generalised linear model in R.

614

615

616

ASSOCIATED CONTENT

Supporting Information (PDF).

The PDF file includes:

- Supplementary text
- Supplemental Materials and Methods
- Figures S1 to S2
- SI References

AUTHOR INFORMATION

Corresponding Author

*Correspondence: Aya Takesono (A.Takesono@exeter.ac.uk) and Charles R. Tyler (c.r.tyler@exeter.ac.uk).

Author Contributions

Conceptualization, A.T., T.K. and C.R.T.; Methodology, A.T., S.D., N.J.C., M.J.W; Formal analysis, A.T. and S.D.; Investigation, A.T., S.D. and N.J.C.; Writing – Original Draft, A.T; Writing – Review & Editing, A.T., S.D., N.J.C., T.K. and C.R.T.; Funding Acquisition, T.K. and C.R.T.; Resources, A.T., S.D., S.M., R.D.H., T.K and C.R.T.; Supervision, A.T. and C.R.T.

All authors have given approval to the final version of the manuscript.

Funding Sources

This work was funded by Natural Environment Research Council, UK (grant reference NE/L007371/1), Biological and Biotechnology Research Council, UK (grant reference BB/L020637/1) and the European Union's Horizon 2020 research and innovation programme under grant agreement No 760813.

ACKNOWLEDGMENT

We are grateful to ARC staff at University of Exeter for husbandry of the zebrafish.

ABBREVIATIONS

AOP, adverse outcome pathway; OS, oxidative stress; ZnONP, zinc oxide nanoparticles; OSNs, the olfactory sensory neurons; MONPs, metal oxide nanomaterials; ROS, reactive oxygen species; NAC, N-acetyl-cysteine; LC_{50}, Lethal Concentration 50**%;** dpf, days post fertilisation; the 3Rs, Replacement, Reduction, and Refinement; EpRE, electrophile response element; OE, the olfactory epithelium; OB, the olfactory bulb; hpf, hours post fertilisation; $EC_{50,}$ The mean effective concentration; KLH, anti-keyhole limpet hemocyanin; mdGs, mediodorsal glomeruli; dlG, dorsolateral glomerulous; ROI, the region of interest; EQS, The environmental quality standard; Pac, a total acoustic power; EDF, extended depth focus; PFA, paraformaldehyde.

REFERENCES

Ache, B.W.; Young, J.M. Olfaction: Diverse Species, Conserved Principles. Neuron 2005;48:417-430

658 Adamcakova-Dodd, A.; Stebounova, L.V.; Kim, J.S.; Vorrink, S.U.; Ault, A.P.; O'Shaughnessy,
659 P.T.; Grassian, V.H.; Thorne, P.S. Toxicity assessment of zinc oxide nanoparticles using
660 sub-acute and sub-chronic murine inhalation models. Part Fibre Toxicol 2014;11:15
661 Affairs., D.f.E.F.R. Water Framework Directive Implementation in
662 England and Wales: New and Updated Standards to Protect the Water Environment. 2014;
663 Azevedo, S.L.; Ribeiro, F.; Jurkschat, K.; Soares, A.M.; Loureiro, S. Co-exposure of ZnO
664 nanoparticles and UV radiation to Daphnia magna and Danio rerio: Combined effects
665 rather than protection. Environ Toxicol Chem 2016;35:458-467
666 Bates, D.M. lme4: Mixed-effects modeling with R. Springer New York; 2010
667 Bonfanti, P.; Moschini, E.; Saibene, M.; Bacchetta, R.; Rettighieri, L.; Calabri, L.; Colombo, A.;
668 Mantecca, P. Do Nanoparticle Physico-Chemical Properties and Developmental
669 Exposure Window Influence Nano ZnO Embryotoxicity in Xenopus laevis? Int J Environ
670 Res Public Health 2015;12:8828-8848
671 Booth, A.a.J., K.A. Protocol for producing reproducible dispersions of manufactured
672 nanomaterials in environmental exposure media. A common European approach to the
673 regulatory testing of nanomaterials, NANoReg 2015;Version 6
674 Brun, N.R.; Lenz, M.; Wehrli, B.; Fent, K. Comparative effects of zinc oxide nanoparticles and
675 dissolved zinc on zebrafish embryos and eleuthero-embryos: importance of zinc ions. Sci
676 Total Environ 2014;476-477:657-666
677 Du, J.; Cai, J.; Wang, S.; You, H. Oxidative stress and apotosis to zebrafish (Danio rerio)
678 embryos exposed to perfluorooctane sulfonate (PFOS) and ZnO nanoparticles.
679 International Journal of Occupational Medicine and Environmental Health 2017;30:213-
680 229
681 Feeney, G.P.; Zheng, D.; Kille, P.; Hogstrand, C. The phylogeny of teleost ZIP and ZnT zinc
682 transporters and their tissue specific expression and response to zinc in zebrafish.
683 Biochimica et Biophysica Acta (BBA) - Gene Structure and Expression 2005;1732:88-95
684 Frederickson, C.J.; Koh, J.Y.; Bush, A.I. The neurobiology of zinc in health and disease. Nat
685 Rev Neurosci 2005;6:449-462
686 Gottschalk, F.; Sonderer, T.; Scholz, R.W.; Nowack, B. Modeled Environmental Concentrations
687 of Engineered Nanomaterials (TiO2, ZnO, Ag, CNT, Fullerenes) for Different Regions.
688 Environmental Science & Technology 2009;43:9216-9222
689 Hara, T.; Takeda, T.A.; Takagishi, T.; Fukue, K.; Kambe, T.; Fukada, T. Physiological roles of
690 zinc transporters: molecular and genetic importance in zinc homeostasis. J Physiol Sci
691 2017;67:283-301
692 Huang, C.-C.; Aronstam, R.S.; Chen, D.-R.; Huang, Y.-W. Oxidative stress, calcium
693 homeostasis, and altered gene expression in human lung epithelial cells exposed to ZnO
694 nanoparticles. Toxicol In Vitro 2010;24:45-55
695 Jacobsen, N.R.; Stoeger, T.; van den Brule, S.; Saber, A.T.; Beyerle, A.; Vietti, G.; Mortensen,
696 A.; Szarek, J.; Budtz, H.C.; Kermanizadeh, A.; Banerjee, A.; Ercal, N.; Vogel, U.;
697 Wallin, H.; Møller, P. Acute and subacute pulmonary toxicity and mortality in mice after
698 intratracheal instillation of ZnO nanoparticles in three laboratories. Food Chem Toxicol
699 2015;85:84-95
700 Jo, S.M.; Won, M.H.; Cole, T.B.; Jensen, M.S.; Palmiter, R.D.; Danscher, G. Zinc-enriched
701 (ZEN) terminals in mouse olfactory bulb. Brain Research 2000;865:227-236

Jordan, A.; Hill, R.; Turner, A.; Roberts, T.; Comber, S. Assessing Options for Remediation of Contaminated Mine Site Drainage Entering the River Teign, Southwest England. Minerals 2020;10:721
Kobayashi, M.; Yamamoto, M. Nrf2-Keap1 regulation of cellular defense mechanisms against electrophiles and reactive oxygen species. Advances in enzyme regulation 2006;46:113-140
Koide, T.; Miyasaka, N.; Morimoto, K.; Asakawa, K.; Urasaki, A.; Kawakami, K.; Yoshihara, Y. Olfactory neural circuitry for attraction to amino acids revealed by transposon-mediated gene trap approach in zebrafish. Proceedings of the National Academy of Sciences 2009;106:9884-9889
Larner, F.; Dogra, Y.; Dybowska, A.; Fabrega, J.; Stolpe, B.; Bridgestock, L.J.; Goodhead, R.; Weiss, D.J.; Moger, J.; Lead, J.R.; Valsami-Jones, E.; Tyler, C.R.; Galloway, T.S.; Rehkämper, M. Tracing Bioavailability of ZnO Nanoparticles Using Stable Isotope Labeling. Environmental Science & Technology 2012;46:12137-12145
Minghetti, M.; Schnell, S.; Chadwick, M.A.; Hogstrand, C.; Bury, N.R. A primary FIsh Gill Cell System (FIGCS) for environmental monitoring of river waters. Aquatic Toxicology 2014;154:184-192
Mittal, M.; Siddiqui, M.R.; Tran, K.; Reddy, S.P.; Malik, A.B. Reactive oxygen species in inflammation and tissue injury. Antioxid Redox Signal 2014;20:1126-1167
Miyasaka, N.; Wanner, A.A.; Li, J.; Mack-Bucher, J.; Genoud, C.; Yoshihara, Y.; Friedrich, R.W. Functional development of the olfactory system in zebrafish. Mechanisms of Development 2013;130:336-346
Monsé, C.; Hagemeyer, O.; Raulf, M.; Jettkant, B.; van Kampen, V.; Kendzia, B.; Gering, V.; Kappert, G.; Weiss, T.; Ulrich, N.; Marek, E.M.; Bünger, J.; Brüning, T.; Merget, R. Concentration-dependent systemic response after inhalation of nano-sized zinc oxide particles in human volunteers. Part Fibre Toxicol 2018;15:8
Mourabit, S.; Fitzgerald, J.A.; Ellis, R.P.; Takesono, A.; Porteus, C.S.; Trznadel, M.; Metz, J.; Winter, M.J.; Kudoh, T.; Tyler, C.R. New insights into organ-specific oxidative stress mechanisms using a novel biosensor zebrafish. Environ Int 2019;133:105138
Naito, W.; Kamo, M.; Tsushima, K.; Iwasaki, Y. Exposure and risk assessment of zinc in Japanese surface waters. Sci Total Environ 2010;408:4271-4284
Niethammer, P.; Grabher, C.; Look, A.T.; Mitchison, T.J. A tissue-scale gradient of hydrogen peroxide mediates rapid wound detection in zebrafish. Nature 2009;459:996-999
Office, H. Use of Standard Genetically Altered (GA) zebrafish (Danio rerio) breeding protocols.
Pérez-Escudero, A.; Vicente-Page, J.; Hinz, R.C.; Arganda, S.; de Polavieja, G.G. idTracker: tracking individuals in a group by automatic identification of unmarked animals. Nat Methods 2014;11:743-748
Plum, L.M.; Rink, L.; Haase, H. The essential toxin: impact of zinc on human health. Int J Environ Res Public Health 2010;7:1342-1365
Radi, A.M.; Abdel Azeem, N.M.; El-Nahass, E.S. Comparative effects of zinc oxide and zinc oxide nanoparticle as feed additives on growth, feed choice test, tissue residues, and histopathological changes in broiler chickens. Environ Sci Pollut Res Int 2021;28:5158-5167
Safar, R.; Doumandji, Z.; Saidou, T.; Ferrari, L.; Nahle, S.; Rihn, B.H.; Joubert, O. Cytotoxicity and global transcriptional responses induced by zinc oxide nanoparticles NM 110 in PMA-differentiated THP-1 cells. Toxicology Letters 2019;308:65-73

748 Saptarshi, S.R.; Feltis, B.N.; Wright, P.F.; Lopata, A.L. Investigating the immunomodulatory
749 nature of zinc oxide nanoparticles at sub-cytotoxic levels in vitro and after intranasal
750 instillation in vivo. J Nanobiotechnology 2015;13:6
751 Schulte, P.A.; Leso, V.; Niang, M.; Iavicoli, I. Current state of knowledge on the health effects
752 of engineered nanomaterials in workers: a systematic review of human studies and
753 epidemiological investigations. Scand J Work Environ Health 2019;45:217-238
754 Sekler, I.; Moran, A.; Hershfinkel, M.; Dori, A.; Margulis, A.; Birenzweig, N.; Nitzan, Y.;
755 Silverman, W.F. Distribution of the zinc transporter ZnT-1 in comparison with chelatable
756 zinc in the mouse brain. J Comp Neurol 2002;447:201-209
757 Sharma, V.; Anderson, D.; Dhawan, A. Zinc oxide nanoparticles induce oxidative DNA damage
758 and ROS-triggered mitochondria mediated apoptosis in human liver cells (HepG2).
759 Apoptosis 2012;17:852-870
760 Shikazono, N.; Zakir, H.M.; Sudo, Y. Zinc contamination in river water and sediments at Taisyu
761 Zn–Pb mine area, Tsushima Island, Japan. Journal of Geochemical Exploration
762 2008;98:80-88
763 Singh, K.; Madhusudanan, M.; Verma, A.K.; Kumar, C.; Ramawat, N. Engineered zinc oxide
764 nanoparticles: an alternative to conventional zinc sulphate in neutral and alkaline soils for
765 sustainable wheat production. 3 Biotech 2021;11:322
766 Sirelkhatim, A.; Mahmud, S.; Seeni, A.; Kaus, N.H.M.; Ann, L.C.; Bakhori, S.K.M.; Hasan, H.;
767 Mohamad, D. Review on Zinc Oxide Nanoparticles: Antibacterial Activity and Toxicity
768 Mechanism. Nano-Micro Letters 2015;7:219-242
769 Strähle, U.; Scholz, S.; Geisler, R.; Greiner, P.; Hollert, H.; Rastegar, S.; Schumacher, A.;
770 Selderslaghs, I.; Weiss, C.; Witters, H.; Braunbeck, T. Zebrafish embryos as an
771 alternative to animal experiments--a commentary on the definition of the onset of
772 protected life stages in animal welfare regulations. Reprod Toxicol 2012;33:128-132
773 Takesono, A.; Kudoh, T.; Tyler, C.R. Application of Transgenic Zebrafish Models for Studying
774 the Effects of Estrogenic Endocrine Disrupting Chemicals on Embryonic Brain
775 Development. Frontiers in Pharmacology 2022a;13
776 Takesono, A.; Schirrmacher, P.; Scott, A.; Green, J.M.; Lee, O.; Winter, M.J.; Kudoh, T.; Tyler,
777 C.R. Estrogens regulate early embryonic development of the olfactory sensory system via
778 estrogen-responsive glia. Development 2022b;149
779 Team, R.C. R: A language and environment for statistical computing. 2013;
780 Vimercati, L.; Cavone, D.; Caputi, A.; De Maria, L.; Tria, M.; Prato, E.; Ferri, G.M.
781 Nanoparticles: An Experimental Study of Zinc Nanoparticles Toxicity on Marine
782 Crustaceans. General Overview on the Health Implications in Humans. Frontiers in
783 Public Health 2020;8
784 Vorkamp, K.S., Hans. . European Environmental Quality Standards (EQS) Variability Study:
785 Analysis of the variability between national EQS values across Europe for selected Water
786 Framework Directive River Basin-Specific Pollutants ed^eds: Aarhus University, DCE –
787 Danish Centre for Environment and Energy © 2016
788 Winter, M.J.; Pinion, J.; Tochwin, A.; Takesono, A.; Ball, J.S.; Grabowski, P.; Metz, J.;
789 Trznadel, M.; Tse, K.; Redfern, W.S.; Hetheridge, M.J.; Goodfellow, M.; Randall, A.D.;
790 Tyler, C.R. Functional brain imaging in larval zebrafish for characterising the effects of
791 seizurogenic compounds acting via a range of pharmacological mechanisms. British
792 Journal of Pharmacology 2021;178:2671-2689

793 Winter, M.J.; Windell, D.; Metz, J.; Matthews, P.; Pinion, J.; Brown, J.T.; Hetheridge, M.J.; Ball,
794 J.S.; Owen, S.F.; Redfern, W.S.; Moger, J.; Randall, A.D.; Tyler, C.R. 4-dimensional
795 functional profiling in the convulsant-treated larval zebrafish brain. Scientific Reports
796 2017;7:6581
797 Wyatt, T.D. Pheromones and animal behaviour : communication by smell and taste. 2003;
798 Xia, T.; Kovochich, M.; Liong, M.; Mädler, L.; Gilbert, B.; Shi, H.; Yeh, J.I.; Zink, J.I.; Nel,
799 A.E. Comparison of the mechanism of toxicity of zinc oxide and cerium oxide
800 nanoparticles based on dissolution and oxidative stress properties. ACS Nano
801 2008;2:2121-2134
802 Yang, Y.; Liu, X.; Luo, L.; Wei, W.; Wang, Q.; Zhang, J. Quantitative Detection of Zinc Oxide
803 Nanoparticle in Environmental Water by Cloud Point Extraction Combined ICP-MS.
804 Adsorption Science & Technology 2021;2021:9958422
805 Yoo, S.K.; Starnes, T.W.; Deng, Q.; Huttenlocher, A. Lyn is a redox sensor that mediates
806 leukocyte wound attraction in vivo. Nature 2011;480:109-112
807 Zhao, X.; Ren, X.; Zhu, R.; Luo, Z.; Ren, B. Zinc oxide nanoparticles induce oxidative DNA
808 damage and ROS-triggered mitochondria-mediated apoptosis in zebrafish embryos.
809 Aquat Toxicol 2016;180:56-70
810 Zhao, X.; Wang, S.; Wu, Y.; You, H.; Lv, L. Acute ZnO nanoparticles exposure induces
811 developmental toxicity, oxidative stress and DNA damage in embryo-larval zebrafish.
812 Aquat Toxicol 2013;136-137:49-59

813